Two-site small polaron quantum states: Optimization of the dressing fraction

Vincent Pouthier*
Institut UTINAM, Université de Franche–Comté, CNRS UMR 6213, 25030 Besançon Cedex, France
(Received 26 March 2009; revised manuscript received 6 May 2009; published 24 June 2009)

A modified Lang-Firsov transformation is used to study the exciton-phonon interaction in a two-site system embedded in a one-dimensional lattice. It describes an exciton partially dressed by a virtual phonon cloud and depends on a single variational parameter, the so-called dressing fraction, whose optimization is achieved by using both the standard Bogoliubov inequality and its improved version defined by Decoster [J. Phys. A **37**, 9051 (2004)]. The optimization procedure is applied to build a phase diagram in the parameter space which defines the different states of the exciton depending on the adiabaticity, the coupling strength, and the temperature. It is shown that the two Bogoliubov inequalities yield different variational principles that give rise to two optimal dressing fractions. Special attention is thus paid to characterize their differences in the nonadiabatic limit, where the exciton evolves continuously from a partially dressed state in the weak-coupling limit to a fully dressed state in the strong-coupling limit, and in the adiabatic limit where a self-trapped transition takes place.

DOI: 10.1103/PhysRevB.79.214304 PACS number(s): 71.35.−y, 71.38.Ht, 71.38.Fp, 63.22.−m

I. INTRODUCTION

Charge and energy transfers between atomic subunits in large molecules and crystals play a key role in understanding various phenomena in both physics, chemistry, and biology.[1] Examples among many are Frenkel excitons in photosynthetic antenna,[2–4] allowing the conversion of solar energy into chemical energy, and vibrons in α helices expected to be at the origin of the transduction of the chemical energy into mechanical work in proteins.[5–11]

Among the different models introduced to study energy transfer, a special attention has been paid to characterize the dynamics provided by a Fröhlich-type (or a Holstein-type) Hamiltonian.[12,13] Such an Hamiltonian gives a general description of the transport of a particle (called an exciton in the following text) coupled with the vibrations of the host medium, which correspond either to acoustical (Fröhlich model) or optical (Holstein model) phonons.

Although this Hamiltonian cannot be solved exactly, it exhibits two asymptotic solutions depending on the values taken by the relevant parameters of the model, i.e., the exciton bandwidth Φ, the phonon cutoff frequency Ω_c, and the small polaron binding energy E_B proportional to the strength of the exciton-phonon coupling. In the adiabatic limit ($\Phi \gg \Omega_c$), the phonons behave in a classical way and create a quasistatic potential well responsible for the trapping of the exciton. Dressed by this lattice distortion, the exciton forms a large polaron whose description contains well-known nonlinearities that arise from either stationary or time-dependent semiclassical variational methods (see, for instance, Ref. 7). By contrast, in the nonadiabatic limit ($\Phi \ll \Omega_c$), the quantum nature of the phonons plays a crucial role. The exciton is dressed by a virtual cloud of phonons which yields a lattice distortion essentially located on a single site and which instantaneously follows the exciton. The exciton dressed by the virtual phonon cloud forms a small polaron whose properties are described by performing the so-called Lang-Firsov (LF) (see Ref. 14) transformation. However, this transformation is not exact and the remaining polaron-phonon coupling is usually addressed by applying a perturbation theory.[8,15–20]

To improve the description of the exciton-phonon system, different strategies have been elaborated during the last four decades. Citing all these works is clearly outside the scope of the present paper and we shall restrict our attention on specific approaches involving the concept of partial dressing. To reach the partially dressed exciton point of view, the main idea is to perform a modified Lang-Firsov (MLF) transformation. This transformation depends on variational parameters that define the so-called dressing fraction. It refers to a partially dressed exciton instead of the fully dressed picture that emerges from the LF transformation. In that context, at zero temperature, the dressing fraction is determined by minimizing the system ground-state energy (see, for instance, Refs. 21–24 and the references inside). To interpolate between the two asymptotic solutions of the Fröhlich Hamiltonian, Brown, Ivic, and coworkers introduced a unified theory whose starting point was also based on the MLF transformation.[25–28] In the partially dressed point of view, a trial quantum state is introduced in analogy with the D_1 Davydov's ansatz.[6] Combining time-dependent variational principles and an average over the phonon degrees of freedom, the dressing fraction is finally optimized by minimizing the system ground-state energy. Based on thermodynamics arguments, a slightly different approach has been developed to extract the temperature dependence of the dressing fraction (see, for instance, Refs. 29–32). This method, which works quite well in the nonadiabatic limit, still involves the MLF transformation. Nevertheless, the optimization step does no longer refer to the system ground-state properties but it is based on the free-energy concept. Indeed, combining the first-order thermodynamical perturbation expansion with both the Jensen inequality for convex functions[33] and the Peierls theorem[34,35] results in an exact upper bound for the system free energy. This feature, known as the Bogoliubov inequality,[36] allows to introduce a trial free energy that depends on the variational parameters and whose minimization yields the optimal dressing fraction.

In the present paper, this latter optimization procedure is revisited by using the so-called "second quantum Bogoliu-

bov inequality" defined by Decoster.[37] In this recent paper, Decoster generalized the Jensen theorem for the exponential function and considered high-order perturbation expansion. Consequently, a new inequality has been established, stronger than the original one, which provides an upper bound for the system free energy lower than the upper bound given by the original Bogoliubov inequality. Therefore, the fundamental question arises whether the improved Bogoliubov inequality modifies the concept of partial dressing. To answer that question, we consider a quantum dimer describing a single exciton delocalized between two nearest-neighbor sites embedded in a lattice. Although this model is rather unrealistic to describe energy transfer, it provides a simple approach to understand clearly the modification of the dressing mechanism. A more realistic model will be presented in forthcoming papers where both size effects and exciton propagation over a lager site number will be discussed.

The paper is organized as follows. In Sec. II, the system Hamiltonian is described and the MLF transformation is defined in terms of the unknown dressing fraction. In Sec. III, the first and the second Bogoliubov inequalities are used to introduce trial free energies that depend on the dressing fraction. Their minimization is performed in Sec. IV to define the optimal dressing fraction whose behavior is analyzed in great details.

II. DESCRIPTION OF THE SYSTEM

A. Model and Hamiltonians

Let us consider a one-dimensional (1D) lattice with fixed boundary conditions and containing N sites $x=1,\ldots,N$. In this lattice, an exciton is able to delocalize between two neighboring sites x_1 and $x_2=x_1+1$. Note that in the present paper we consider the situation of large N values for which x_1 is about $N/2$. Let $|i\rangle$ denote the quantum state occupied by the exciton located on the x_ith site. The exciton Hamiltonian H_e is thus expressed as

$$H_e = \sum_{i=1,2} \omega_0 |i\rangle\langle i| + \Phi[|1\rangle\langle 2| + |2\rangle\langle 1|], \tag{1}$$

where ω_0 is the energy of the state $|i\rangle$ and where Φ is the hopping constant.

The dimer interacts with the acoustical phonons of the lattice whose Hamiltonian is written as

$$H_p = \sum_{x=1}^{N} \frac{p_x^2}{2M} + \sum_{x=1}^{N-1} \frac{W}{2}(u_{x+1}-u_x)^2 + \frac{W}{2}(u_1^2+u_N^2). \tag{2}$$

In Eq. (2), M is the mass of each site whose external displacement and momentum are u_x and p_x, respectively, and W is the lateral force constant between nearest-neighbor sites. Due to the fixed boundary conditions, a stationary regime takes place and the phonon eigenstates correspond to N normal modes with quantized wave vectors $q_p=p\pi/L$, with $p=1,\ldots,N$ and $L=N+1$. The corresponding frequencies are $\Omega_p=\Omega_c \sin(p\pi/2L)$, where $\Omega_c=\sqrt{4W/M}$. Within this normal-mode representation, the phonon Hamiltonian is rewritten in terms of the standard phonon operators $a_p^\dagger$ and a_p as $H_p=\Sigma_{p=1}^{N}\Omega_p(a_p^\dagger a_p+1/2)$.

The exciton-phonon interaction is given by the potential deformation model in which the lattice dynamics gives rise to random fluctuations of each dimer site energy. Within the normal-mode decomposition of the phonon field, the corresponding Hamiltonian is written as[38]

$$\Delta H_{ep} = \sum_{p,i} \Delta_{p,i}(a_p^\dagger + a_p)|i\rangle\langle i|, \tag{3}$$

where $\Delta_{p,i}$ is expressed in terms of the small polaron binding energy E_B as

$$\Delta_{p,i} = 2\sqrt{\frac{E_B\Omega_c}{L}}\sin(q_p/2)^{1/2}\cos(q_p/2)\cos(q_p x_i). \tag{4}$$

The exciton-phonon dynamics is thus described by the full Hamiltonian $H=H_e+H_p+\Delta H_{ep}$.

B. Partially dressed exciton point of view

To reach the partially dressed exciton point of view, a two-step procedure is applied. First, we define the MLF transformation in terms of the dressing fraction η, as

$$U(\eta) = \exp\left[\eta \sum_{p,i} \frac{\Delta_{p,i}}{\Omega_p}(a_p^\dagger - a_p)|i\rangle\langle i|\right]. \tag{5}$$

Equation (5) is a simplified version of a more general transformation that involves a set of p-dependent variational parameters η_p. We thus assume $\eta_p=\eta, \forall p$, which strongly simplifies the optimization procedure and gives qualitatively the same results as p-dependent methods.[25]

From Eq. (5), the transformed Hamiltonian $\hat{H}(\eta)=U(\eta)HU^\dagger(\eta)$ is expressed as

$$\hat{H}(\eta) = \sum_i \hat{\omega}_0(\eta)|i\rangle\langle i| + \Phi[\Theta_1^\dagger\Theta_2|1\rangle\langle 2| + \text{H.c.}] + \sum_{p,i}(1-\eta)\Delta_{p,i}(a_p^\dagger + a_p)|i\rangle\langle i| + H_p, \tag{6}$$

where H.c. denotes the Hermitian conjugate. In Eq. (6), $\hat{\omega}_0(\eta)=\omega_0-\eta(2-\eta)\epsilon_B$, where $\epsilon_B=E_B(1-2/L)$, and $\Theta_i=\langle i|U^\dagger(\eta)|i\rangle$ denotes the dressing operator.

The next step of the procedure consists in expressing $\hat{H}(\eta)$ as the sum of three separated contributions, i.e., $\hat{H}(\eta)=H_{po}(\eta)+H_p+\Delta H(\eta)$. To proceed, an average $\langle\ldots\rangle_p$ over the phonon degrees of freedom in thermal equilibrium at temperature T is performed. The polaron Hamiltonian $H_{po}(\eta)=\langle\hat{H}(\eta)-H_p\rangle_p$ is thus defined as

$$H_{po}(\eta) = \sum_i \hat{\omega}_0(\eta)|i\rangle\langle i| + \hat{\Phi}(\eta)[|1\rangle\langle 2| + |2\rangle\langle 1|]. \tag{7}$$

In Eq. (7), $\hat{\Phi}(\eta)=\Phi\langle\Theta_1^\dagger\Theta_2\rangle_p=\Phi\exp[-\eta^2 S(T)]$ involves the coupling constant $S(T)$ defined as

$$S(T) = \frac{8E_B}{L\Omega_c}\sum_p \sin(q_p/2)\cos^2(q_p/2)\sin^2(q_p\bar{x})f_p, \tag{8}$$

where $\bar{x}=(x_1+x_2)/2$ and $f_p=\coth(\beta\Omega_p/2)$ ($\beta=1/k_BT$ with k_B is the Boltzmann constant). Finally, the polaron-phonon interaction $\Delta H(\eta)$ is written as

$$\Delta H(\eta) = [\Phi\Theta_1^+\Theta_2 - \hat{\Phi}(\eta)]|1\rangle\langle 2| + \text{H.c.} + \sum_{p,i}(1-\eta)\Delta_{p,i}(a_p^\dagger + a_p)|i\rangle\langle i|. \quad (9)$$

At this step, Eq. (7) allows us to express the different operators in the polaronic eigenstate basis. These eigenstates are delocalized over the two sites of the dimer. They correspond to a symmetric and an antisymmetric superimposition of the local states, as $|\pm\rangle = (|1\rangle \pm |2\rangle)/\sqrt{2}$. The corresponding eigenenergies are defined as $\omega_\pm(\eta) = \hat{\omega}_0(\eta) \pm \hat{\Phi}(\eta)$. Within this representation, the coupling $\Delta H(\eta)$ is defined as

$$\Delta H(\eta) = \begin{pmatrix} \Delta\omega + V & \delta\omega - \delta V \\ \delta\omega + \delta V & \Delta\omega - V \end{pmatrix}, \quad (10)$$

where

$$\Delta\omega(\eta) = \frac{1-\eta}{2}\sum_p \Delta_p(a_p^\dagger + a_p),$$

$$\delta\omega(\eta) = \frac{1-\eta}{2}\sum_p \delta\Delta_p(a_p^\dagger + a_p),$$

$$V(\eta) = \frac{\Phi}{2}\{T + T^\dagger - 2\exp[-\eta^2 S(T)]\},$$

$$\delta V(\eta) = \frac{\Phi}{2}[T - T^\dagger], \quad (11)$$

with $\Delta_p = \Delta_{p1} + \Delta_{p2}$, $\delta\Delta_p = \Delta_{p1} - \Delta_{p2}$, and $T = \Theta_1^\dagger\Theta_2$.

From this point of view, $H_{po}(\eta)$ describes the dynamics of an exciton partially dressed by a lattice distortion. Its delocalization between the two sites of the dimer is characterized by the effective hopping constant $\hat{\Phi}(\eta)$ which is smaller than the bare constant Φ. Moreover, the dressing yields a redshift of each site energy. Because the MLF transformation is not exact, a polaron-phonon coupling remains and two contributions occur. First, due to the incomplete nature of the transformation, random fluctuations of each site energy still contribute to the interaction. Then, the phonon dynamics yields a modulation of the hopping term through the dressing-operator fluctuations. Consequently, the question arises how to choose the dressing fraction η, which still remains unknown. This is a fundamental question since, depending on the relevant parameters of the model, the answer allows us to formulate the best strategy to study the exciton-phonon dynamics and treat the remaining coupling. Therefore, in the next section, thermodynamics arguments will be invoked to optimize the dressing fraction according to both the standard Bogoliubov theorem and its improved version.

III. UPPER BOUNDS OF THE FREE ENERGY

A. First Bogoliubov inequality

In this section, the optimal η value is determined according to the standard Bogoliubov theorem. To proceed, we assume that the exciton-phonon system is in thermal equilibrium at temperature T. Its statistical state is described by the canonical density matrix, so that the corresponding free energy is defined as $\mathcal{F} = -k_B T \ln\{Tr[\exp(-\beta H)]\}$. As an observable, the free energy is independent on the point of view and it can be expressed in terms of the transformed Hamiltonian as

$$\mathcal{F} = -k_B T \ln[Tr\{\exp[-\beta\hat{H}(\eta)]\}], \quad (12)$$

where $\mathcal{F}$ remains η independent.

At this step, let us define $\hat{H}(\eta) = H_0(\eta) + \Delta H(\eta)$, where $H_0(\eta) = H_{po}(\eta) + H_p$ is the unperturbed Hamiltonian. We thus denote $\langle\ldots\rangle_0$ the average according to the canonical density matrix associated to $H_0(\eta)$. As a result, the Bogoliubov theorem states that the exact free energy of the exciton-phonon system exhibits an upper bound defined as

$$\mathcal{F} \leq \mathcal{F}_0(\eta) + \langle\Delta H(\eta)\rangle_0, \quad (13)$$

where $\mathcal{F}_0(\eta) = -k_B T \ln[Tr\{\exp[-\beta H_0(\eta)]\}]$. The Bogoliubov theorem provides a variational principle to define the optimal dressing fraction as the η value, which minimizes the right-hand side of Eq. (13). Since $\langle\Delta H\rangle_0 = 0$, the knowledge of both the polaronic eigenstates and the phonon properties allow us to determine $\mathcal{F}_0(\eta)$ easily. Therefore, disregarding terms η independent, it is straightforward to show that the optimization step requires the minimization of the following trial free energy:

$$F_0(\eta) = \hat{\omega}_0(\eta) - k_B T \ln[\cosh(\beta\hat{\Phi}(\eta))]. \quad (14)$$

Equation (14) defines the mean-field (MF) model free energy whose minimization yields the optimal dressing fraction η_0. It is given by the transcendental equation written as

$$\eta = \left\{1 + \frac{\hat{\Phi}(\eta)S(T)}{\epsilon_B}\tanh[\beta\hat{\Phi}(\eta)]\right\}^{-1} \quad (15)$$

At zero temperature, Eq. (15) reduces to the equation that optimizes the dressing fraction according to the ground-state minimization procedure introduced by Brown and Ivic [see Eq. (4.17) in Ref. 25 with the corresponding $B(T) \to \Phi S(T=0)/\epsilon_B$]. By contrast, when the temperature exceeds the exciton bandwidth, Eq. (15) reduces to $\eta = 1/[1 + \beta\hat{\Phi}^2(\eta)S(T)/\epsilon_B]$. We thus recover the result obtained by Brown and Ivic but with the corresponding $S(T) \to 2S(T)$ and $B(T) \to \Phi^2\beta S(T)/\epsilon_B$.

B. Second Bogoliubov inequality

Decoster recently improved the standard Bogoliubov procedure and obtained a series of exact upper bounds for a system free energy by combining high-order perturbation theory with a generalization of the Jensen inequality for the convex exponential function.[37] In this paper, we consider the upper bound that arises from a third-order perturbation expansion. It is defined by the second Bogoluibov inequality, as

$$\mathcal{F} \leq \mathcal{F}_0(\eta) + \langle \Delta H(\eta) \rangle_0 - \frac{1}{\beta} \ln \left[1 + \frac{\beta^2 v_2}{2} e^{-\beta v_3 / 3 v_2} \right]. \tag{16}$$

Given that $\langle \Delta H \rangle_0 = 0$, $v_2(\eta)$ and $v_3(\eta)$ are expressed as

$$v_2(\eta) = \langle \Delta H(\eta)^2 \rangle_0,$$

$$v_3(\eta) = \langle \Delta H(\eta)^3 + \Delta H(\eta)[H_0(\eta), \Delta H(\eta)] \rangle_0. \tag{17}$$

Disregarding terms independent of η, Eq. (16) yields a variational principle to optimize the dressing fraction by minimizing the following trial free energy:

$$F_1(\eta) = F_0(\eta) - k_B T \ln \left[1 + \frac{\beta^2 v_2}{2} e^{-\beta v_3 / 3 v_2} \right]. \tag{18}$$

Equation (18) defines the corrected mean-field (CMF) model free energy whose minimum is reached for the optimal dressing fraction η_1.

After performing fastidious but straightforward calculations, Eqs. (10) and (11) have been used to determine $v_2(\eta)$ and $v_3(\eta)$. To proceed, a thermal average over the phonon degrees of freedom has been done with the help of the formula listed in the Appendix. One finally obtains

$$v_2(\eta) = \Phi^2 (1 - e^{-2\eta^2 S}) - \eta(1-\eta) E_B \hat{\Phi} \tanh(\beta \hat{\Phi}) + \frac{(1-\eta)^2}{4} \sum_p [\Delta_p^2 + \delta \Delta_p^2] \coth\left(\frac{\beta \Omega_p}{2} \right) \tag{19}$$

and

$$v_3(\eta) = \left[\frac{1-\eta}{2} \Omega_c \right]^2 E_B + \eta E_B \Phi^2 [1 - 3(1-\eta) e^{-2\eta^2 S}] + 2\hat{\Phi} \tanh(\beta \hat{\Phi}) \Phi^2 [1 - e^{-2\eta^2 S}] + \frac{1}{2}(1-\eta)(1-3\eta) \hat{\Phi} \tanh(\beta \hat{\Phi}) \sum_p \delta \Delta_p^2 \coth\left(\frac{\beta \Omega_p}{2} \right) - \frac{3}{4} \eta^2 (1-\eta)^2 E_B^2 \hat{\Phi} \tanh(\beta \hat{\Phi}), \tag{20}$$

where the η dependence of $\hat{\Phi}(\eta)$ has been omitted to simplify the notation.

Equations (14) and (18) are the main results of the present paper. They define trial free energies $F_0(\eta)$ and $F_1(\eta)$ whose minimization yields the optimal dressing fractions η_0 and η_1, respectively. In the next section, the minimization procedure is performed numerically and special attention is paid to characterize the behavior of both η_0 and η_1 depending on the temperature and the relevant parameters of the model.

IV. NUMERICAL RESULTS AND DISCUSSION

To study the optimal dressing fraction, reduced parameters are introduced. First, let $B = 2\Phi / \Omega_c$ denote the adiabaticity which measures the ratio between the exciton velocity and the phonon velocity. Then, one defines the parameter $C = E_B / \Omega_c$ as the strength of the exciton-phonon interaction.

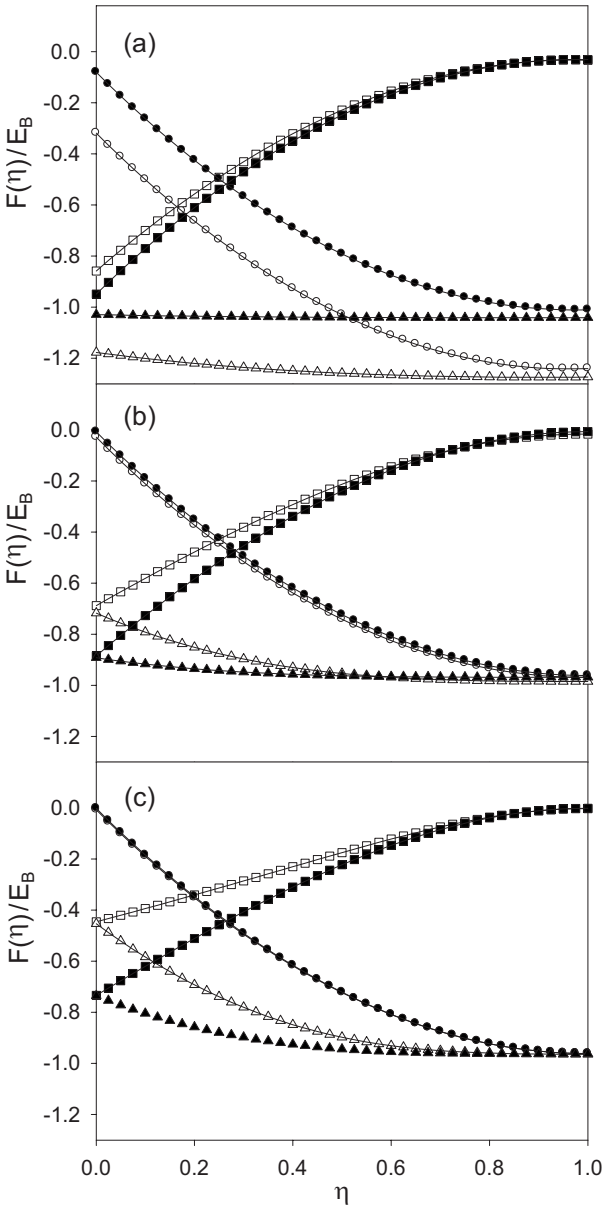

FIG. 1. Free energies $F_0(\eta)/E_B$ (circles), $\Delta F(\eta)/E_B$ (squares), and $F_1(\eta)/E_B$ (triangles) for $B=0.2$, $\theta=0.5$ (open symbols), and $\theta=2.0$ (full symbols). (a) $C=0.0312$, (b) $C=0.3465$, and (c) $C=1.3862$.

Finally, let $\theta = k_B T / \Omega_c$ be the reduced temperature. Note that the lattice size is fixed to $L=52$ and $x_1 = L/2$.

In that context, we first focus our attention on the behavior of the optimal dressing fraction in the nonadiabatic limit, i.e., for small B values. Such a situation occurs in several physical problems and an example among many is given by the vibron-phonon dynamics in α helices. In that case, B ranges between 0.1 and 0.3 whereas an uncertainty on the coupling remains, so that C can be viewed as a free parameter.[39]

The η dependence of $F_0(\eta)$, $F_1(\eta)$, and $\Delta F(\eta) = F_1(\eta) - F_0(\eta)$ is illustrated in Fig. 1 for $B=0.2$ and $\theta=0.5$ (open symbols), and $\theta=2.0$ (full symbols). Whatever C and θ be, Fig. 1 shows that $F_1(\eta)$ is a slowly varying function of the dressing fraction. It is less sensitive to η than $F_0(\eta)$ which

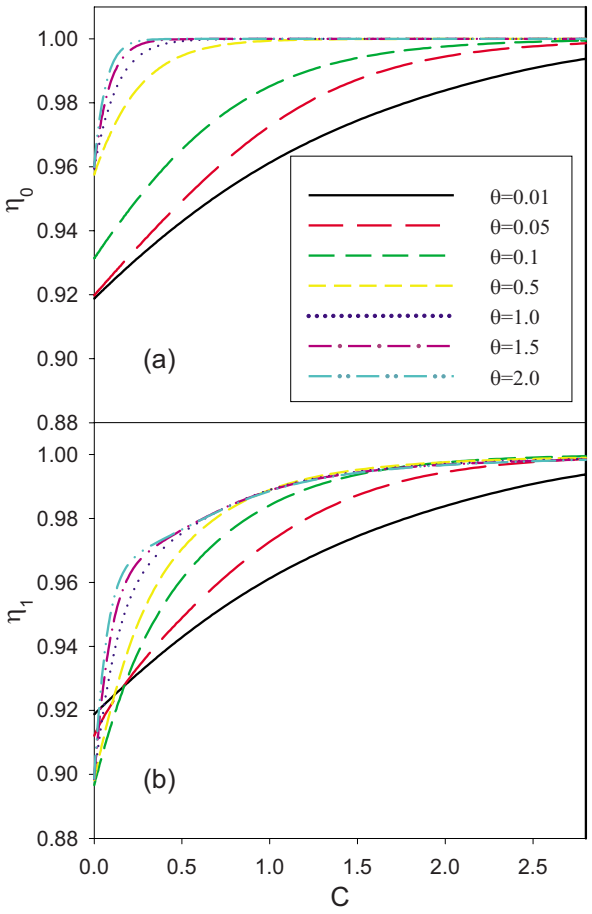

FIG. 2. (Color online) Optimal dressing fraction (a) η_0 and (b) η_1 for $B=0.2$ and for different values of the reduced temperature.

exhibits a rather important η dependence. This effect is particularly pronounced for small C values and at high temperature. To measure this effect, let $\delta F_i = F_i(0) - F_i(\eta_i)$ denote the difference between the maximum and the minimum of $F_i(\eta)$. In the weak-coupling limit [Fig. 1(a)], $\delta F_0/E_B \approx 0.925$ is almost temperature independent. By contrast, $\delta F_1/E_B$ is more than one order of magnitude smaller and it decreases with the temperature. It is equal to 0.097 for $\theta=0.5$ and reduces to 0.012 for $\theta=2.0$. Figures 1(b) and 1(c) reveal that $\delta F_0/E_B \approx 0.945$ is almost θ and C independent. In a marked contrast, $\delta F_1/E_B$ increases with C and decreases with θ.

Nevertheless, Fig. 1 shows that $\Delta F(\eta)$ strongly depends on η. It takes a significant negative value for small η values but it increases and finally almost vanishes when η reaches unity. Such a behavior is fundamental because in the nonadiabatic limit, the optimal dressing fraction is close to unity within both the MF and the CMF model (see Fig. 2). Consequently, although $F_0(\eta)$ varies significantly with η, its minimum is close to the minimum of $F_1(\eta)$. To illustrate this feature, let $\Delta F_o = F_0(\eta_0) - F_1(\eta_1)$ denote the difference between the minimum of the two trial free energies. In the weak-coupling limit [Fig. 1(a)], $\Delta F_o/E_B$ is about 0.031 whatever θ be. By contrast, as displayed in Figs. 1(b) and 1(c), $\Delta F_o/E_B$ decreases with both C and θ. For instance, for $C=1.38$, it varies from 0.003 for $\theta=0.5$ to 0.001 for $\theta=2.0$.

The C dependence of η_0 and η_1 is illustrated in Fig. 2 for $B=0.2$. Within the MF model, $\eta_0(C)$ is a slowly varying function of the coupling strength C [Fig. 2(a)]. It increases with C to rapidly converge to unity. This behavior is well described by the exponential increase $\eta_0(C) \approx 1 + [\eta_o - 1]\exp(-\gamma C)$ where both η_o and γ depend on the temperature. At low temperature $\eta_o \approx 0.918 (\theta < 0.05)$ but it slightly increases with the temperature to finally reach 0.959 at high temperature. By contrast, γ scales as $\gamma \approx 0.52 + 7.36\theta$, indicating that the higher the temperature, the faster the convergence of $\eta_0(C)$.

TABLE I. Parameters for the multiexponential fit of the free-energy difference $(\delta F/E_B) \times 10^4$.

θ	a	b	c	d	g	h
0.5	3.466	7.440	3.434	7.440	2.151	2.402
1.0	2.067	12.717	0.456	2.203	0.031	0.749
2.0	0.077	36.022	0.491	21.715	0.092	1.516

As shown in [Fig. 2(b)], $\eta_1(C)$ behaves as $\eta_0(C)$ at very low temperature only. When $\theta < 0.05$, $\eta_1(C=0)$ is about 0.918 and when the coupling is turned on, $\eta_1(C)$ converges to unity, according to an exponential increase. However, at higher temperature, a different behavior takes place. First, $\eta_1(C=0)$ decreases with the temperature to finally converge to 0.898. Then, when C is turned on, $\eta_1(C)$ still increases with C to reach unity, but it no longer follows the exponential law. A slowing down in its increase occurs so that all the curves tend to coincide whatever be the temperature. It is, as if, $\eta_1(C)$ was unable to penetrate a forbidden region. This slowing-down effect is clearly evidenced at high temperature. For instance, when $\theta=1$, 1.5, and 2.0, $\eta_1(C)$ first increases according to an exponential law until C reaches typically 0.3. Then, the three curves behave similarly and develop almost the same C dependence. The main consequence is that the convergence of $\eta_1(C)$ is slower than the convergence of $\eta_0(C)$ at high temperature. Therefore, η_1 is always smaller than η_0 indicating that the CMF model favors a less-efficient dressing than the MF model. Nevertheless, in the nonadiabatic limit, the difference between the two optimal dressing fractions remains rather small.

At this step, the C dependence of $\delta F = F_1(1) - F(\eta_1)$ has been studied for different temperature to obtain information about the free-energy difference between the fully dressed point of view and the partially dressed point of view. Our study reveals that $\delta F/E_B$ is a very small parameter which decreases with the temperature. It is smaller than 10^{-3} at low temperature $(\theta=0.5)$ and this upper bound reaches 10^{-4} at high temperature $(\theta=2)$. The behavior of $\delta F/E_B$ is well described by a multiexponential decay defined as

$$\delta F/E_B = a\exp(-bC) + c\exp(-dC) + g\exp(-hC), \tag{21}$$

where the different parameters are listed in Table I. Since C is proportional to E_B, Eq. (21) shows that δF tends to zero when C vanishes. Then, as C increases, δF increases ($\delta F \propto C$ for small C values) until it reaches a maximum value. This maximum is equal to $2.9 \times 10^{-4} E_B$, $7.5 \times 10^{-5} E_B$, and $3.6 \times 10^{-6} E_B$ when $\theta=0.5$, 1, and 2, respectively. Its succes-

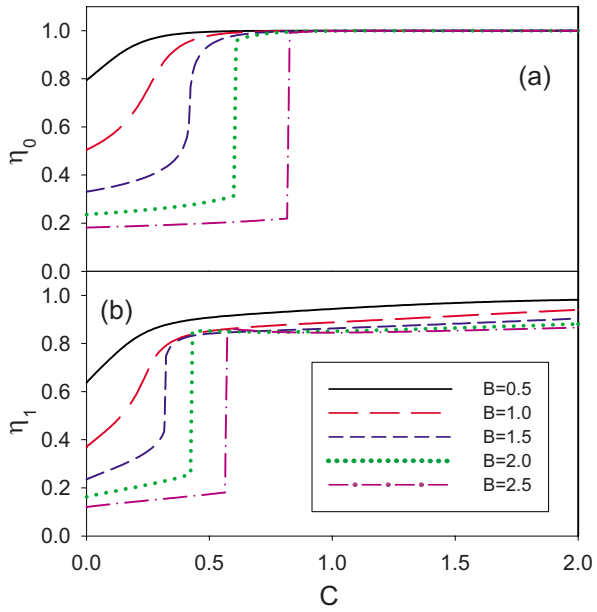

FIG. 3. (Color online) Optimal dressing fraction (a) η_0 and (b) η_1 for $\theta=1.0$ and for different B values.

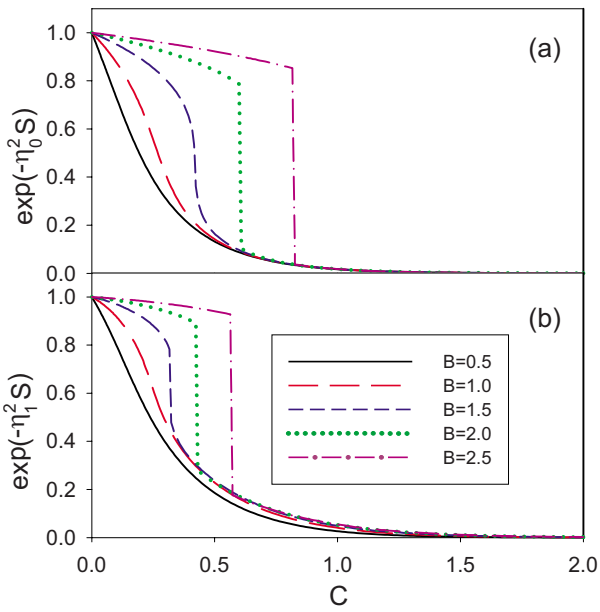

FIG. 4. (Color online) Dressing factor (a) $\exp(-\eta_0^2 S)$ and (b) $\exp(-\eta_1^2 S)$ for $\theta=1.0$ and for different B values.

sively occurs for $C=0.19$, 0.13, and 0.62. Finally, for larger C values, δF decreases by exhibiting a behavior dominated by an exponential decay. These results clearly suggest that within the nonadiabatic limit, the full-dressing approach works quite well provided the exciton-phonon coupling is accounted according to, at least, a third-order perturbation theory.

The influence of the adiabaticity on the optimal dressing fraction is illustrated in Fig. 3 for $\theta=1.0$. When B increases from the nonadiabatic limit, i.e., for $B=0.5$ and 1.0, the optimal dressing fraction still remains a continuous slowly varying function of the coupling that finally converges to unity. However, the influence of the adiabaticity is twofold. First, in the weak-coupling limit, both η_0 and η_1 are decaying functions of B which indicates that the adiabaticity reduces the dressing. Then, the larger the adiabaticity, the longer the convergence of the optimal dressing fraction when C increases. This feature is more pronounced within the CMF model and [Fig. 3(b)] reveals that η_1 converges very slowly for both $B=0.5$ and $B=1.0$. Note that, as in the nonadiabatic limit, η_1 is always smaller than η_0 for a fixed set of the parameters B, C, and θ.

A fully different behavior takes place for larger B values. Indeed, when $B=1.5$, $\eta_1(C)$ exhibits a discontinuity for a critical value of the coupling equal to $C^*(B=1.5)=0.323$ and it realizes a jump from 0.435 to 0.746. In fact, around the discontinuity, the trial free energy $F_1(\eta)$ shows a double well indicating the occurrence of two minima and one maximum. When $C<C^*(B)$, the absolute minimum takes place for a small η value whereas it occurs for a large η value when $C>C^*(B)$. Consequently, an unstable state is reached at the critical point, i.e., for $C=C^*(B)$, since the two minima of the trial free energy become equal. As displayed in [Fig. 3(b)], a discontinuity is observed for $B=2$ and $B=2.5$ for $C^*(B=2)=0.432$ and $C^*(B=2.5)=0.569$, respectively.

As shown in [Fig. 3(a)], similar features characterize $\eta_0(C)$. Nevertheless, the discontinuity in $\eta_0(C)$ does not take place for the same set of parameters. For instance, no instability is observed for $B=1.5$ and the curve remains continuous. A discontinuity appears for both $B=2.0$ and $B=2.5$, and it occurs for $C^*(B=2)=0.608$ and $C^*(B=2.5)=0.823$, respectively. Moreover, for a given B value, η_0 is always greater than η_1, before and after the discontinuity. For instance, for $B=2.0$, η_0 realizes a jump between 0.313 and 0.958 whereas η_1 performs a jump between 0.257 and 0.851.

The discontinuity of the dressing fraction for a sufficiently large adiabaticity is a well-known effect which has been described in details in previous papers (see, for instance, Refs. 25 and 29, and the references inside). As illustrated in Fig. 4, which represents the C dependence of the ratio between the optimal-effective hopping constant $\hat{\Phi}(\eta_i)$ and the bare hopping constant Φ, this effect characterizes the so-called self-trapped transition which discriminates between two states for the exciton. When $C<C^*(B)$, the exciton is weakly dressed and it almost refers to a bare exciton whose effective hopping constant is close to Φ. By contrast, when $C>C^*(B)$, the exciton is almost fully dressed. It is characterized by a very small effective hopping constant which reveals its strong self-localized nature. In other words, the exciton is almost trapped in a local state due to the dressing.

The key point in the present approach is that the CMF model softens the transition when compared with the standard MF approach. The origin of this softening is twofold. First, for a fixed B value, the CMF critical coupling $C^*(B)$ is always smaller than the MF one. Therefore, the CMF transition occurs for a smaller value of the coupling constant S [see Eq. (8)]. Then, as mentioned previously, η_1 is always smaller than η_0 around their corresponding discontinuity. The main consequence is that, just before and just after the transition, $\hat{\Phi}(\eta_1)$ is always larger than $\hat{\Phi}(\eta_0)$. In other words, in the almost bare state, the CMF model softens the dressing effect whereas in the self-trapped state, it reduces the localized nature of the exciton. For instance, for $B=2.5$, $\hat{\Phi}(\eta_1)$

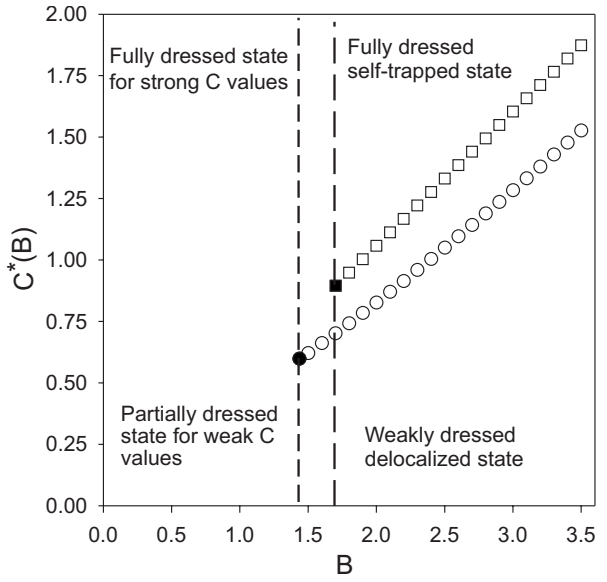

FIG. 5. Phase diagram in the parameter space for $\theta=0.5$. Squares define the MF critical curve whereas circles refer to the CMF critical curve. Full symbols denote the critical points.

varies between 0.927Φ and 0.176Φ at the transition. By contrast, the MF model yields a jump in $\hat{\Phi}(\eta_0)$ from 0.852Φ to 0.036Φ.

As shown in previous figures, a transition takes place when the adiabaticity exceeds a critical value B^* for a given temperature. Therefore, simulations at different temperatures have been carried out to extract the behavior of the so-called critical curve which is illustrated in Fig. 5 for $\theta=0.5$. Circles refer to the CMF model whereas squares characterize the MF model. This critical curve defines a phase diagram in the parameter space which discriminates between different states of the exciton. It is characterized by the critical point, i.e., the beginning of the curve, whose coordinates are defined by B^* and $C^*=C^*(B^*)$ (full symbols). When $B<B^*$, no transition takes place so that the state of the exciton evolves continuously from a partially dressed state for weak C values to a fully dressed state for strong C values. By contrast, when $B>B^*$, a transition occurs and the critical curve discriminates between the almost bare state when $C<C^*(B)$ and the self-trapped state when $C>C^*(B)$.

Figure 5 reveals that the phase diagrams provided by both the CMF model and the MF model are slightly different. First, we have verified that the CMF critical curve is always below the MF critical curve, whatever the temperature. Then, the coordinates of the critical point also differ. For instance, for $\theta=0.5$, $B^*=1.435$, and $C^*=0.598$ for the CMF model whereas the MF approach yields $B^*=1.702$ and $C^*=0.895$. More precisely, the CMF critical curve follows a power law, as

$$C^*(B) - C^* = K(B - B^*)^{\alpha}, \tag{22}$$

where both K and α depend on θ. When $0<\theta<0.3$, K is typically about 0.5 whereas the exponent α is close to unity. The critical curve clearly behaves as a line segment. At higher temperature, the exponent α slightly increases to finally converge around 1.3–1.4. By contrast, the parameter K decreases with the temperature and it scales as $K\approx 0.24/\theta$ when $\theta>1$.

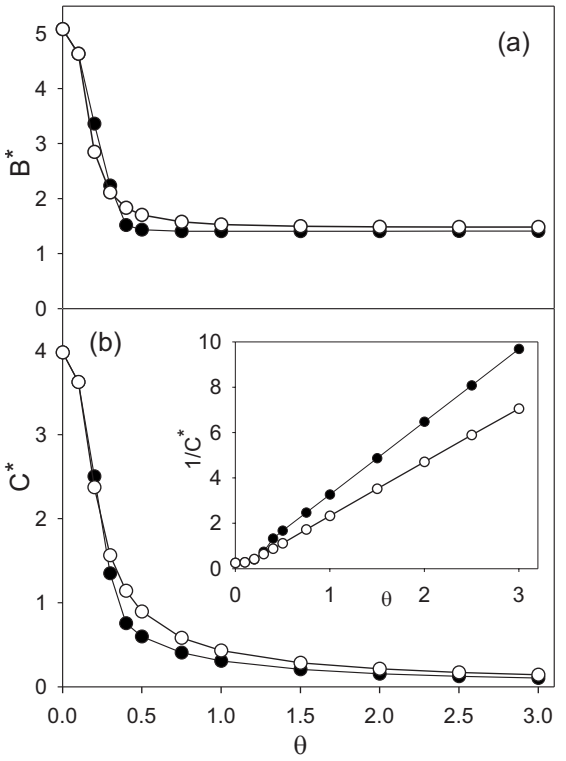

FIG. 6. Temperature dependence of the critical point (a) B^* and (b) C^* for both the CMF model (full symbols) and the MF model (open symbols).

Finally, the temperature dependence of the critical point is displayed in Fig. 6. The behavior of the CMF critical point strongly depends on the temperature and two regimes occur (full circles). At high temperature ($\theta>0.5$), $B^*(\theta)\approx 1.40$ is almost temperature independent. By contrast, when $\theta<0.5$, $B^*(\theta)$ suddenly increases when θ decreases. It finally converges to $B^*(0)\approx 5.08$ at zero temperature. Such temperature dependence is well described by a Gaussian law defined as

$$B^*(\theta) = B^*(\infty) + [B^*(0) - B^*(\infty)]\exp[-(\theta^2/\theta_0)^2], \tag{23}$$

where $\theta_0\approx 0.25$. As shown in [Fig. 6(b)], the behavior of the critical coupling is also dominated by two regimes depending on whether the temperature is high or low. At high temperature, $C^*(\theta)$ decreases with the temperature and it scales as $C^*(\theta)\approx 0.31/\theta$. By contrast, in the low-temperature limit, a slowing down in the increase in $C^*(\theta)$ occurs when the temperature decreases. The critical coupling does no longer behave as $1/\theta$, but it typically scales as $C^*(\theta)\approx C^*(0)/[1+(\theta/\theta_0)^3]$. It finally converges to a finite value of about $C^*(0)\approx 3.97$ at zero temperature.

Similar features are observed for the θ dependence of the MF critical point (open circles). Indeed, at high temperature, $B^*(\theta)\approx 1.48$ whatever θ is, whereas $C^*(\theta)$ follows the invert law $C^*(\theta)\approx 0.42/\theta$. In the low-temperature limit, $B^*(\theta)$ increases when θ decreases and $C^*(\theta)$ does no longer follow the invert law. In fact, Fig. 6 clearly shows that the MF

critical point converges to the CMF critical point at zero temperature. These results can be recovered with the help of Eq. (15) whose solution yields the optimal η value within the MF approach. Indeed, this equation is similar to the transcendental equation introduced by Brown and Ivic to define the optimal dressing fraction by minimizing the exciton ground-state energy in an infinite lattice [see Eq. (4.17) in Ref. 25]. This equation yields a phase diagram in the parameter space which describes a first-order phase transition whose critical point is expressed in terms of the two parameters $B^*(T)=1/2e^{3/2}$ and $S^*(T)=27/8$. In that context, at zero temperature, Eq. (15) reduces to that of Brown and Ivic's with the corresponding $B(T)\rightarrow\Phi S(T=0)/\epsilon_B$ and $S(T=0)=3\pi C/8$. It yields critical-point coordinates in a perfect agreement with the observed features as

$$B^*(0)=\frac{3\pi}{8}\left(1-\frac{2}{L}\right)e^{3/2}\approx 5.08,$$

$$C^*(0)=\frac{81\pi}{64}\approx 3.97, \tag{24}$$

where the L dependence originates from the definition of ϵ_B [see Eq. (6)]. By contrast, when the temperature exceeds the exciton bandwidth, we recover the result of Brown and Ivic, but with the corresponding $S(T)\rightarrow 2S(T)$ and $B(T)\rightarrow\Phi^2\beta S(T)/\epsilon_B$. Therefore, given that $S(T)\approx 4C\theta$ at high temperature, Eq. (15) yields the critical-point coordinates as

$$B^*(\theta)=\sqrt{\frac{1}{2}\left(1-\frac{2}{L}\right)e^{3/2}}\approx 1.47,$$

$$C^*(\theta)=\frac{27}{64}\frac{1}{\theta}\approx\frac{0.42}{\theta}. \tag{25}$$

Equation (25) clearly reproduces the numerical results displayed in Fig. 6 for the MF model.

The similitudes between the behavior of both the CMF critical point and the MF critical point, combined with the analytical results given by Eq. (15), show that the temperature dependence of the critical point originates from the temperature dependence of the population of the polaronic eigenstates. Indeed, the population difference between the polaronic eigenstates is defined as $\tanh[\beta\hat{\Phi}(\eta)]$ (see Eq. (15)). When the temperature exceeds the exciton bandwidth, this factor behaves as $\hat{\Phi}(\eta)/k_BT$. It, thus, cancels the temperature dependence of the term $\Phi S(T)/\epsilon_B$ and yields an almost temperature-independent critical adiabaticity. By contrast, when the temperature decreases, the population difference tends to unity, indicating that only the ground state is significantly populated at low temperature. Therefore, both the CMF model and the MF model converge to the same approach in which the optimal dressing fraction arises from the ground-state properties.

To conclude this section, let us mention that the CMF model is based on the equal dressing-fraction assumption. The influence of the exciton-phonon coupling is thus captured in a single variational parameter η that defines the MLF transformation ($\eta_p=\eta\forall p$). This parameter is optimized in accordance with the second Bogoliubov inequality so that the CMF model provides a better characterization of the polaron Hamiltonian than the standard MF model. Nevertheless, other variational procedures have been elaborated and the fundamental question arises whether the CMF model is more accurate than these methods. In particular, we could expect that variational methods involving a set of p-dependent dressing fractions η_p yield better results than the CMF model.

In a general way, the implementation of such methods is very difficult because it requires the minimization of a trial free energy with respect to a large number of variational parameters. To overcome this difficulty, Ivic and coworkers have recently introduced a variational method to study the behavior of the effective tunneling frequency in a spin-boson system.[40] In this method, a judicious change of variables allows the authors to define a set of p-dependent dressing fractions η_p in terms of a single variational parameter a. This change in variables results from an anticipation of the explicit form of the optimized η_p values obtained in accordance with the standard Bogoliubov inequality.

In that context, we have applied the method of Ivic *et al.* to our exciton-phonon Hamiltonian that slightly differs from the spin-boson Hamiltonian. Therefore, a trial free energy $F_2(a)$ is built by using the standard Bogoliubov theorem and its minimization is performed to define the optimal value of the effective hopping constant $\hat{\Phi}_2$. By comparing the minimum of the CMF trial free energy F_1 and the minimum of the trial free energy F_2, we have observed that a critical value of the coupling strength $C_0(B,\theta)$ discriminates between two situations. When $C<C_0(B,\theta)$, the CMF model is more accurate than the Ivic procedure since it yields an upper bound for the exact system free energy, which is lower than the upper bound given by the Ivic model. By contrast, the reverse situation occurs when $C>C_0(B,\theta)$. The key point is that the critical value $C_0(B,\theta)$ strongly depends on both B and θ. To illustrate this feature, calculations have been carried out for $\theta=1.0$. In the nonadiabatic limit, i.e., when $B=0.2$, C_0 vanishes indicating that the Ivic model is more accurate than the CMF model. However, both models yield almost identical values for the free-energy upper bound provided that C is smaller than 0.01. Moreover, they lead to similar optimal effective hopping constants whatever C is. When $B=0.5$, the accuracy of the CMF model prevails provided that C is smaller than $C_0=0.65$. However, when $C>C_0$, both models still give rise to similar effective hopping constants since $[\hat{\Phi}(\eta_1)-\hat{\Phi}_2]/\Phi$, which is always smaller than 3×10^{-2}, rapidly converges to zero as C increases. Such a behavior is enhanced when $B=1.0$, since $C_0=1.77$. When $C>C_0$, $[\hat{\Phi}(\eta_1)-\hat{\Phi}_2]/\Phi$ remains smaller 10^{-3} and it rapidly vanishes as C increases. Finally, when $B=1.5$ and $B=2.0$, C_0 reaches 2.80 and 3.67, respectively. In that case, the CMF model clearly prevails over the Ivic model and it allows for a complete description of the self-trapping transition.

Consequently, these results show that in the nonadiabatic limit, the CMF model is more accurate than the Ivic model in the weak-coupling limit only. However, as C increases, both models yield similar optimal effective hopping constants. By contrast, in the adiabatic limit, the CMF model is more ac-

curate than the Ivic model over a wide range of coupling strength. Nevertheless, these features depend on the temperature, and more detailed calculations will be performed in a forthcoming paper to clearly define the domain of validity of each model.

V. CONCLUSION

In the present paper, a MLF transformation has been used to analyze the exciton-phonon interaction in a two-site system embedded in a 1D lattice. Instead of the fully dressed picture that emerges from the LF transformation, the MLF transformation describes an exciton partially dressed by a virtual phonon cloud. It depends on a single variational parameter, the so-called dressing fraction η, whose optimization has been achieved by using both the standard Bogoliubov theorem (MF model) and its improved version defined by Decoster (CMF model). The optimization procedure has been used to define a phase diagram in the parameter space which discriminates between the different states of the exciton depending on the relevant parameters of the problem, i.e., the adiabaticity B, the coupling strength C, and the reduced temperature θ. Similar to a first-order phase transition, this diagram exhibits a critical curve whose beginning defines the so-called critical point (B^*, C^*).

When $B < B^*$, no transition takes place so that the state of the exciton evolves continuously from a partially dressed state for weak C values to a fully dressed state for strong C values. In the nonadiabatic limit $(B \ll 1)$, it has been shown that the CMF model gives rise to a better approximate to the exact system free energy than the MF model. Nevertheless, at low temperature, both the MF and the CMF models yield similar optimal dressing fractions, labeled η_0 and η_1, which are slowly varying functions of C. They are both close to unity in the weak-coupling limit and increase with C to finally reach unit in the strong-coupling limit. As the temperature increases, η_0 still behaves as before, but the higher the temperature, the faster its convergence. By contrast, a slowing down in the increase of η_1 takes place which results in a very slow convergence to unity in the strong-coupling limit and yields $\eta_1 < \eta_0$.

When $B > B^*$, a transition takes place. It is characterized by the occurrence of a discontinuity in the optimal dressing fraction when the coupling reaches a critical value $C^*(B)$. When $C < C^*(B)$, the exciton is weakly dressed and it is delocalized over the two sites of the dimer. By contrast, when $C > C^*(B)$, the full dressing induces a localization of the exciton which is self-trapped in a local state. It has been shown that the corrections which arise in the CMF model modify the properties of the transition. First, the CMF model softens the transition when compared with the standard MF approach. Indeed, within the CMF model, the localized nature of the exciton is reduced in the self-trapped state whereas the effective hopping constant is enhanced in the almost delocalized bare state. Then, the CMF critical curve is always below the MF critical curve indicating that for a given B value, the CMF critical coupling is smaller than the MF one. Finally, in the high-temperature limit, the CMF critical adiabaticity equal to 1.40 is smaller than the MF one of about 1.48. However, as the temperature decreases, both critical values increase to finally converge to the same value at zero temperature. Such a behavior originates from the temperature dependence of the population of the polaronic eigenstates and, at very low temperature, both the CMF and the MF models converge to the same approach in which the optimal dressing fraction arises from the minimization of the ground- state energy.

To conclude, let us mention that special attention will be paid in forthcoming papers to address two fundamental questions. First, we have shown that the CMF model provides a good estimate of the polaron Hamiltonian although it is based on the assumption of an equal dressing for all phonon modes. Nevertheless, additional studies are required to clearly establish the domain of validity of such a model when compared with other approaches, especially those involving p-dependent dressing fractions as introduced in Ref. 40. Then, the present approach must be generalized to describe more realistic systems in which the exciton is able to delocalize over a larger site number. In that case, the polaronic eigenstates do no longer refer to a two-level system but define a continuous energy band. Therefore, the calculation of the ingredients that enter the present formalism will be more difficult and we expect the occurrence of modified Bessel function instead of the standard hyperbolic functions. Moreover, the temperature will affect the behavior of the critical curves in a different way, especially when it will be about the exciton bandwidth.

APPENDIX: AVERAGES OVER THE PHONON DEGREES OF FREEDOM

In this appendix, specific averages are evaluated to determine the parameters involved in the second Bogoliubov inequality. To proceed, let us first define the centered translation operator $\mathcal{T}(\alpha_p)$, whose average over the phonon degrees of freedom vanishes, as

$$\mathcal{T}(\alpha_p) = \exp\left[\sum_p \alpha_p (a_p^\dagger - a_p)\right] - \exp[-\mathcal{S}], \qquad \text{(A1)}$$

where $\mathcal{S} = 1/2 \Sigma_p \alpha_p^2 \coth(\beta\Omega_p/2)$. Then, let $\mathcal{V} = [\mathcal{T}(\alpha_p) + \mathcal{T}^\dagger(\alpha_p)]/2$ and $\delta\mathcal{V} = [\mathcal{T}(\alpha_p) - \mathcal{T}^\dagger(\alpha_p)]/2$ denote the Hermitian part and the anti-Hermitian part of the translation operator, respectively. Finally, let $X_p = a_p^\dagger + a_p$ define the pth phonon coordinate. As shown in Eq. (11), the coupling Hamiltonian $\Delta H(\eta)$ can be expressed in terms of the operators $\mathcal{V}$, $\delta\mathcal{V}$, and X_p. Consequently, to evaluate $v_2(\eta)$ and $v_3(\eta)$ [Eq. (17)], one needs the knowledge of the average over the phonon degrees of freedom of specific contributions involving the product between these different operators.

Disregarding vanishing terms, contributions involving the product between two operators are defined as

$$\langle X_p X_{p'} \rangle_p = \delta_{pp'} \coth(\beta\Omega_p/2),$$

$$\langle \mathcal{V}^2 \rangle_p = (1 - e^{-2\mathcal{S}})^2/2,$$

$$\langle \delta\mathcal{V}^2 \rangle_p = -(1 - e^{-4\mathcal{S}})/2,$$

$$\langle X_p \delta\mathcal{V}\rangle_p = \alpha_p e^{-\mathcal{S}},$$

$$\langle \delta\mathcal{V} X_p\rangle_p = -\alpha_p e^{-\mathcal{S}}. \quad \text{(A2)}$$

Similarly, terms involving the product between three operators are defined as

$$\langle X_p X_{p'} \mathcal{V}\rangle_p = \alpha_p \alpha_{p'} e^{-\mathcal{S}},$$

$$\langle \mathcal{V} X_p X_{p'}\rangle_p = \alpha_p \alpha_{p'} e^{-\mathcal{S}},$$

$$\langle X_p \mathcal{V} X_{p'}\rangle_p = -\alpha_p \alpha_{p'} e^{-\mathcal{S}},$$

$$\langle \mathcal{V} X_p \delta\mathcal{V}\rangle_p = \alpha_p (1 - e^{-2\mathcal{S}}),$$

$$\langle \delta\mathcal{V} X_p \mathcal{V}\rangle_p = -\alpha_p (1 - e^{-2\mathcal{S}}),$$

$$\langle \mathcal{V}\delta\mathcal{V} X_p\rangle_p = \alpha_p e^{-2\mathcal{S}}(1 - e^{-2\mathcal{S}}),$$

$$\langle \delta\mathcal{V}\mathcal{V} X_p\rangle_p = \alpha_p e^{-2\mathcal{S}}(1 - e^{-2\mathcal{S}}),$$

$$\langle X_p \mathcal{V}\delta\mathcal{V}\rangle_p = -\alpha_p e^{-2\mathcal{S}}(1 - e^{-2\mathcal{S}}),$$

$$\langle X_p \delta\mathcal{V}\mathcal{V}\rangle_p = -\alpha_p e^{-2\mathcal{S}}(1 - e^{-2\mathcal{S}}). \quad \text{(A3)}$$

Finally, third-order contributions involving either $\mathcal{V}$ or $\delta\mathcal{V}$ are written as

$$\langle \mathcal{V}^3\rangle_p = e^{-\mathcal{S}}(1 - e^{-4\mathcal{S}})^2/4 - e^{-\mathcal{S}}(1 - e^{-2\mathcal{S}})^2,$$

$$\langle \mathcal{V}\delta\mathcal{V}^2\rangle_p = e^{-\mathcal{S}}(1 - e^{-4\mathcal{S}})^2/4,$$

$$\langle \delta\mathcal{V}^2\mathcal{V}\rangle_p = e^{-\mathcal{S}}(1 - e^{-4\mathcal{S}})^2/4,$$

$$\langle \delta\mathcal{V}\mathcal{V}\delta\mathcal{V}\rangle_p = e^{-\mathcal{S}}(1 - e^{-4\mathcal{S}})^2/4. \quad \text{(A4)}$$

With the help of Eqs. (A2)–(A4), Eq. (17) can be solved to finally obtain Eqs. (19) and (20).

*vincent.pouthier@univ-fcomte.fr

[1] V. May and O. Kuhn, *Charge and Energy Transfer Dynamics in Molecular Systems* (Wiley-VCH Verlag, Berlin, 2000).
[2] T. Renger, V. May, and Oliver Kuhn, Phys. Rep. **343**, 137 (2001).
[3] V. Sundstrom, Prog. Quantum Electron. **24**, 187 (2000).
[4] T. Meier, Y. Zhao, V. Chernyak, and S. Mukamel, J. Chem. Phys. **107**, 3876 (1997).
[5] A. S. Davydov and N. I. Kisluka, Phys. Status Solidi B **59**, 465 (1973); Zh. Eksp. Teor. Fiz. **71**, 1090 (1976) [Sov. Phys. JETP **44**, 571 (1976)].
[6] A. C. Scott, Phys. Rep. **217**, 1 (1992).
[7] W. Forner, Int. J. Quantum Chem. **64**, 351 (1997).
[8] V. Pouthier, Phys. Rev. E **78**, 061909 (2008).
[9] V. Pouthier and Y. O. Tsybin, J. Chem. Phys. **129**, 095106 (2008).
[10] D. Tsivlin and V. May, Chem. Phys. **338**, 150 (2007).
[11] P. A. S. Silva and L. Cruzeiro, Phys. Rev. E **74**, 021920 (2006).
[12] H. Fröhlich, Adv. Phys. **3**, 325 (1954).
[13] T. Holstein, Ann. Phys. (N.Y.) **8**, 325 (1959); Ann. Phys. (N.Y.) **8**, 343 (1959).
[14] I. G. Lang and Yu. A. Firsov, Sov. Phys. JETP **16**, 1293 (1962).
[15] M. Grover and R. Silbey, J. Chem. Phys. **54**, 4843 (1971).
[16] R. Silbey and R. W. Munn, J. Chem. Phys. **72**, 2763 (1980).
[17] R. W. Munn and R. Silbey, J. Chem. Phys. **83**, 1843 (1985); **83**, 1854 (1985).
[18] V. Capek and I. Barvik, J. Phys. C **20**, 1459 (1987).
[19] H. Dolderer and M. Wagner, J. Chem. Phys. **108**, 261 (1998).
[20] V. Pouthier, Physica D **221**, 13 (2006); Physica D **237**, 106 (2008).
[21] G. Venzl and S. F. Fischer, J. Chem. Phys. **81**, 6090 (1984).
[22] G. Venzl and S. F. Fischer, Phys. Rev. B **32**, 6437 (1985).
[23] Z. Lu and H. Zheng, Phys. Rev. B **75**, 054302 (2007).
[24] Z. D. Chen and H. Wong, Phys. Rev. B **78**, 064308 (2008).
[25] D. W. Brown and Z. Ivic, Phys. Rev. B **40**, 9876 (1989).
[26] D. Kostic, Z. Ivic, D. Kapor, M. Lalic, and A. Tancic, Phys. Rev. B **50**, 13315 (1994).
[27] Z. Ivic, G. P. Tsironis, D. Kostic, and M. Lalic, J. Phys.: Condens. Matter **8**, 157 (1996).
[28] Z. Ivic, D. Kostic, Z. Przulj, and D. Kapor, J. Phys.: Condens. Matter **9**, 413 (1997).
[29] D. Yarkony and R. Silbey, J. Chem. Phys. **65**, 1042 (1976).
[30] D. R. Yarkony and R. Silbey, J. Chem. Phys. **67**, 5818 (1977).
[31] R. Silbey and R. A. Harris, J. Chem. Phys. **80**, 2615 (1984).
[32] Z. Przulj, D. Cevizovic, S. Zekovic, and Z. Ivic, Chem. Phys. Lett. **462**, 213 (2008).
[33] J. L. W. V. Jensen, Acta Math. **30**, 175 (1906).
[34] R. Peierls, Phys. Rev. **54**, 918 (1938).
[35] D. ter Haar, Rev. Mod. Phys. **27**, 289 (1955).
[36] M. Girardeau, J. Math. Phys. **3**, 131 (1962).
[37] A. Decoster, J. Phys. A **37**, 9051 (2004).
[38] V. Pouthier, Phys. Rev. E **75**, 061910 (2007).
[39] V. Pouthier, J. Phys.: Condens. Matter **21**, 185404 (2009).
[40] Z. Ivic, D. Kostic, and D. Kapor, Phys. Lett. A **339**, 393 (2005).